

t_1^x	t_1^z	t_2^x	t_2^z	t_3^{xz}
-0.483	-0.110	0.069	-0.017	0.239
t_\perp^x	t_\perp^z	t_4^{xz}	ϵ^x	ϵ^z
0.005	-0.635	-0.034	0.776	0.409

TABLE I. Tight-binding parameters of the bilayer two-orbital model. The hoppings t are demonstrated in Fig. 2a. ϵ^x, ϵ^z are site energies for Ni- $d_{x^2-y^2}, d_{3z^2-r^2}$ orbitals, respectively.

band structure, we arrive at an effective bilayer two-orbital model

$$\begin{aligned}
\mathcal{H} &= \mathcal{H}_0 + \mathcal{H}_U, \\
\mathcal{H}_0 &= \sum_{\mathbf{k}\sigma} \Psi_{\mathbf{k}\sigma}^\dagger H(\mathbf{k}) \Psi_{\mathbf{k}\sigma}, \\
\mathcal{H}_U &= U \sum_{is} n_{is\uparrow} n_{is\downarrow} \\
&\quad + \sum_{i\alpha\beta} (U' - J\delta_{\alpha\beta}) (n_{iA\alpha} n_{iA\beta} + n_{iB\alpha} n_{iB\beta}).
\end{aligned} \tag{1}$$

Here \mathcal{H}_0 is the tight-binding Hamiltonian determined out of our Wannier downfolding, and \mathcal{H}_U is the Coulomb interaction term [46]. The basis is defined as $\Psi_\sigma = (d_{Ax\sigma}, d_{Az\sigma}, d_{Bx\sigma}, d_{Bz\sigma})^T$, with the field operator $d_{s\sigma}$ denotes annihilation of an $s = Ax, Az, Bx, Bz$ electron with spin σ . As shown in Fig. 2, A, B label the bilayer, and x, z label $d_{x^2-y^2}, d_{3z^2-r^2}$ orbitals, respectively. For \mathcal{H}_U , U, U', J are intra-orbital, inter-orbital Coulomb repulsion and Hund coupling, respectively. The matrix $H(\mathbf{k})$ is written as

$$\begin{aligned}
H(\mathbf{k}) &= \begin{pmatrix} H_A(\mathbf{k}) & H_{AB}(\mathbf{k}) \\ H_{AB}(\mathbf{k}) & H_A(\mathbf{k}) \end{pmatrix}, \\
H_A(\mathbf{k}) &= \begin{pmatrix} T_{\mathbf{k}}^x & V_{\mathbf{k}} \\ V_{\mathbf{k}} & T_{\mathbf{k}}^z \end{pmatrix}, \quad H_{AB}(\mathbf{k}) = \begin{pmatrix} t_\perp^x & V_{\mathbf{k}}' \\ V_{\mathbf{k}}' & t_\perp^z \end{pmatrix}. \tag{2}
\end{aligned}$$

with

$$\begin{aligned}
T_{\mathbf{k}}^{x/z} &= 2t_1^{x/z} (\cos k_x + \cos k_y) + 4t_2^{x/z} \cos k_x \cos k_y + \epsilon^{x/z}, \\
V_{\mathbf{k}} &= 2t_3^{xz} (\cos k_x - \cos k_y), \quad V_{\mathbf{k}}' = 2t_4^{xz} (\cos k_x - \cos k_y).
\end{aligned}$$

Here $T_{\mathbf{k}}^{x/z}$ represents intra-layer intra-orbital hopping, and $V_{\mathbf{k}} (V_{\mathbf{k}}')$ represent intra-layer (inter-layer) hybridization between $d_{x^2-y^2}$ and $d_{3z^2-r^2}$ orbitals. The essential hoppings $t_1^{x/z}, t_2^{x/z}, t_3^{xz}, t_4^{xz}$ are demonstrated in Fig. 2a. Note that the minus sign appeared in the structure factor of t_3^{xz}, t_4^{xz} is associated to the orbital symmetry of two e_g sectors.

To better illustrate the low-energy state, it is advisable to further simplify the above model. Recall that the mirror symmetry of the bilayer structure allows us to define the bonding and anti-bonding states $\Phi_{\pm\mathbf{k}\sigma} = (c_{\pm\mathbf{k}\sigma}^x, c_{\pm\mathbf{k}\sigma}^z)^T$ with $c_{\pm\mathbf{k}\sigma}^{x/z} = \frac{1}{\sqrt{2}} (d_{\mathbf{k}A\sigma}^{x/z} \pm d_{\mathbf{k}B\sigma}^{x/z})$, in which

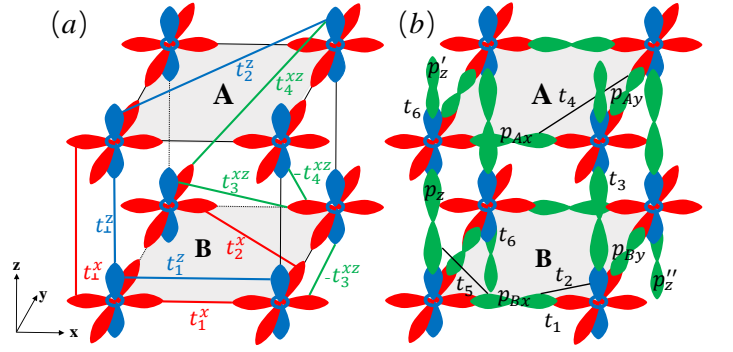


FIG. 2. Schematic of the bilayer $\text{La}_3\text{Ni}_2\text{O}_7$ lattice with hopping parameters. (a) Only Ni- $d_{x^2-y^2}$ (red), $d_{3z^2-r^2}$ (blue) orbitals are shown. The blue, red, green lines indicate hoppings for the bilayer two-orbital model. Their values are listed in Table I. (b) Extra O- p orbitals are drawn as green shapes, with in-plane p_x, p_y and apical p_z, p'_z, p''_z . Some of the p'_z, p''_z are hidden for clarity. The hopping parameters are given in Table II.

the Hamiltonian acquires a block-diagonal form

$$\begin{aligned}
\mathcal{H}_0 &= \sum_{\mathbf{k}\sigma} \left(\Phi_{+\mathbf{k}\sigma}^\dagger H_+(\mathbf{k}) \Phi_{+\mathbf{k}\sigma} + \Phi_{-\mathbf{k}\sigma}^\dagger H_-(\mathbf{k}) \Phi_{-\mathbf{k}\sigma} \right), \\
H_\pm(\mathbf{k}) &= \begin{pmatrix} T_{\mathbf{k}}^x \pm t_\perp^x & V_{\mathbf{k}} \pm V_{\mathbf{k}}' \\ V_{\mathbf{k}} \pm V_{\mathbf{k}}' & T_{\mathbf{k}}^z \pm t_\perp^z \end{pmatrix}. \tag{3}
\end{aligned}$$

In this representation, the two $d_{3z^2-r^2}$ states at E_F are manifested as the component $T_{\mathbf{k}}^z \pm t_\perp^z$ which define a splitting energy $2t_\perp^z$.

With the value of tight-binding parameters listed in Table I, we show in Fig. 3 the resulting band structure and Fermi surface. The model reproduces the DFT band structure well at E_F . Also, site energies are slightly adjusted to coincide with the nominal $d^7.5$ configuration [1, 32]. In Fig. 3b we can see two electron pockets α, β and one hole pocket γ . The α, β -pocket show mixing of orbital content, while the γ -pocket is featured as a dominated $d_{3z^2-r^2}$ state. Note that the amplitude of $t_\perp^z = -0.635$ is even larger than that of the intra-layer nearest-neighbor hopping $t_1^x = -0.483$, by a ratio of 1.3. This strong inter-layer coupling indicates a possible different situation of the unconventional pairing as compared to cuprates, and is in reminiscent of a theoretical bilayer-Hubbard model [47, 48], in which an s_\pm -wave pairing could be promoted via inter-layer coupling. But there is a key difference here. In $\text{La}_3\text{Ni}_2\text{O}_7$, t_\perp^z only appears in $d_{3z^2-r^2}$ sector, while for $d_{x^2-y^2}$ the amplitude $t_\perp^x = 0.005$ is marginal. Hence, the influence from inter-layer coupling to NiO_2 plane can only be achieved via hybridizations $V_{\mathbf{k}}, V_{\mathbf{k}}'$. It would be interesting to see how pairing symmetry is affected in this situation. We would also like to point out that, however, due to the asymmetry of orthorhombic structure of this compound, the γ -pocket from DFT is slightly stretched along nodal direction.

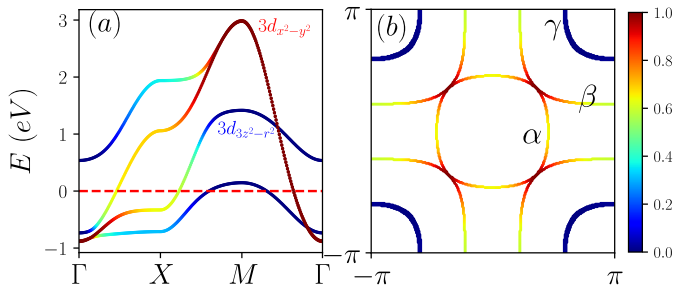


FIG. 3. The band structure (a) and Fermi surface (b) of the bilayer two-orbital model. The colorbar indicates the orbital weight of $d_{x^2-y^2}$ and $d_{3z^2-r^2}$.

t_1	t_2	t_3	t_4	t_5	t_6
-1.564	0.747	-1.625	0.577	-0.487	1.366
ϵ^x	ϵ^z	$\epsilon_p^{x/y}$	ϵ_p^z	$\epsilon_{p'/p''}^z$	
-1.057	-1.161	-4.936	-4.294	-3.772	

TABLE II. Tight-binding parameters for Wannier downfolding of the eleven-orbital model. $\epsilon^{x/z}$ are site energies for $d_{x^2-y^2}/d_{3z^2-r^2}$, and $\epsilon_p^{x/y}$ for in-plane p_x/p_y , and $\epsilon_{p'/p''}^z$ for apical $p_z/p'_z/p''_z$. See Fig. 2b for details.

To explicitly consider the physics of O- p orbitals, we introduce a higher energy model (eleven-orbital model). The basis is $\Psi = (d_{Ax}, d_{Az}, d_{Bx}, d_{Bz}, p_{Ax}, p_{Ay}, p_{Bx}, p_{By}, p_z, p'_z, p''_z)^T$, with four more in-plane $p_{Ax}, p_{Ay}, p_{Bx}, p_{By}$ and three apical p_z, p'_z, p''_z as shown in Fig. 2b. The tight-binding parameters of the model are listed in Tabel II, which requires six hopping parameters including necessary pd, pp overlaps. The resulting band structure covers an energy range akin to that of Fig. 1 and can also reproduced the main features at E_F . Moreover, we found a strong hopping of $t_6 = 1.366$ between $d_{3z^2-r^2}$ and two apical p'_z, p''_z that lie outside the bilayer, which manifest as two hole baths for NiO₂ plane and could be further integrated out in a Löwdin downfolding technique [49]. The model will be useful for further study of the electronic correlation in the dynamic mean field theory framework.

Spin susceptibility.—To determine the magnetic response of the material, we investigate the the spin susceptibility of our model, which is defined as

$$\chi_S^{st}(q, i\omega_n) = \frac{1}{3} \int_0^\beta d\tau e^{i\omega_n \tau} \langle S_s(q, \tau) \cdot S_t(-q, 0) \rangle. \quad (4)$$

Here $s, t = Ax, Az, Bx, Bz$ label orbitals, and the spin operator is defined as $S_{qs} = \frac{1}{2} \sum_{k\alpha\beta} d_{ks\alpha}^\dagger \boldsymbol{\sigma}_{\alpha\beta} d_{k+qs\beta}$ with $\boldsymbol{\sigma}$ the Pauli matrix. By using wick theorem, we expand Eq. 4 to obtain the bare (non-interacting) susceptibility

$$\chi_S^{st}(q, i\omega_n) = -\frac{1}{2N} \sum_{mn} \frac{f(\epsilon_k^n) - f(\epsilon_k^m)}{i\omega_n + \epsilon_k^n - \epsilon_{k+q}^m} \times \langle m|k+qt\rangle \langle k+qs|m\rangle \langle n|ks\rangle \langle kt|n\rangle,$$

with m, n the band indices and $f(\epsilon) = \frac{1}{e^{\epsilon/T} + 1}$ the Fermi-Dirac function. $\langle ks|m\rangle$ represents the eigenvector relating s, m states at wave vector k .

Under the random phase approximation, the spin susceptibility is calculated by

$$\chi_S^{st, \text{RPA}}(q, i\omega_n) = [I - \chi_S^{st}(q, i\omega_n)\Gamma]^{-1} \chi_S^{st}(q, i\omega_n), \quad (5)$$

with interaction vertex defined as

$$\Gamma = \begin{pmatrix} 1 & \\ & 1 \end{pmatrix} \otimes \begin{pmatrix} U & J/2 \\ J/2 & U \end{pmatrix}.$$

In Fig. 4 we show the constant energy slices of $\chi_S^{\text{RPA}}(q, \omega = 0)$. Here we use $U = 3, J = 0.4$ eV. $T = 0$ is applied since temperature only trivially brings a broadening to the spectrum. Fig. 4a is the total $\chi_S^{\text{RPA}} = \sum_{s,t} \chi_S^{st, \text{RPA}}$ corresponding to experimental measurable. As can be seen, the magnetic signal shows a ring-like enhancement. To unveil the origin, we show in Figs. 4b-d the orbital-resolved $\chi_S^{st, \text{RPA}}$, from which we can see a dominated intra-orbital $d_{3z^2-r^2}$ scattering reflecting Fermi surface nesting of γ -pocket. While the signal from other two channels are weaker, consisting with the strong orbital mixing in α, β -pockets. Our result could be further tested in the magnetic measurement.

Discussion.—The discovery of the high transition temperature superconductor La₃Ni₂O₇ represents a major breakthrough in the field of nickletate superconductivity. Our DFT calculations demonstrate that there are two electron pockets α, β and one hole pocket γ on the Fermi surface, in which the α, β -pockets exhibit mixing of orbitals, while the γ -pocket features a dominated $d_{3z^2-r^2}$ content. In comparison to the bulk Ni-112, which has not yet demonstrated a finite T_c , La₃Ni₂O₇ exhibits several distinguishing features that may be crucial to superconductivity. First, the less correlated La-5d derived bands are expelled from the Fermi level, diminishing the hybridization between the Ni- $3d_{x^2-y^2}$ and La-5d orbitals that impedes superconductivity. Furthermore, the site energy difference between Ni- $d_{x^2-y^2}$ and O- p in La₃Ni₂O₇ is estimated as $\Delta \equiv \epsilon_d - \epsilon_p = 3.88$ eV. This value is smaller than that of RNiO₂ (4.4 eV) [16], which could potentially contribute to the high T_c in La₃Ni₂O₇ in the context of pairing based on Zhang-Rice singlet state [50]. The inclusion of the $d_{3z^2-r^2}$ near Fermi level in La₃Ni₂O₇, however, may have complex implications for superconductivity. The large density of state of $d_{3z^2-r^2}$ orbital can provide new phase space for the potential pairing of electrons [51]. However, the presence of multiple orbitals on Fermi level may also lead to competition

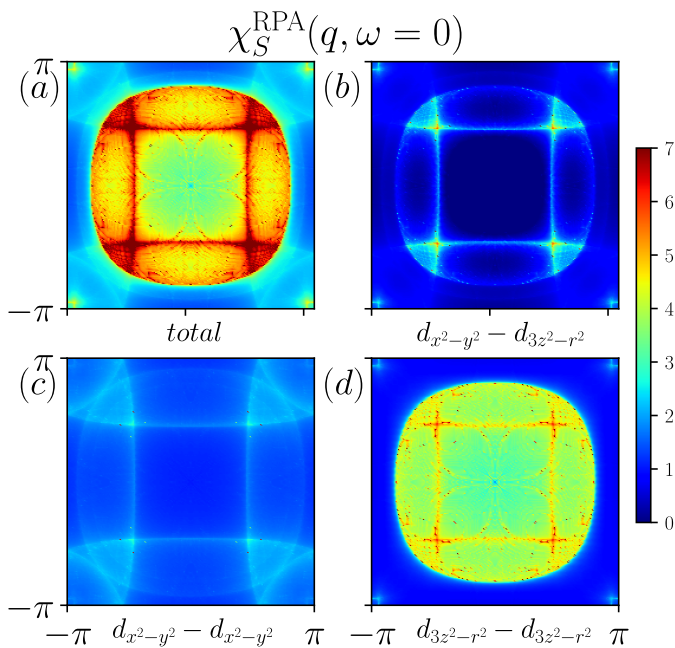


FIG. 4. Spin susceptibility $\chi_S^{st,RPA}(q, \omega = 0)$ of the bilayer two-orbital model. (a) The total orbital sum $\chi_S^{RPA} = \sum_{st} \chi_S^{st,RPA}$ which corresponds to the experimental measurable. (b-d) Orbital-resolved $\chi^{st,RPA}$. An amplified factor of 2 is used in (b-c).

between pairings with different symmetries, such as the competition between $d_{x^2-y^2}$ and s_{\pm} wave pairing. Regarding the filling factors of the relevant orbitals, we note that in the case of a $d^{7.5}$ configuration of Ni, if $d_{3z^2-r^2}$ is considered to roughly have the same occupation number of $d_{x^2-y^2}$, then both orbitals have about 0.75 electrons per site, corresponding to 25% hole-doping. It is notable that the oxygen-deficient in realistic materials may effectively reduce the hole doping level in e_g orbitals of Ni-3d, resulting enhanced superconductivity. Finally, we acknowledge that the $d_{3z^2-r^2}$ orbitals exhibit much weaker hybridization with in-plane oxygen compared to its $d_{x^2-y^2}$ counterpart, which necessitates in-depth investigations into its strong interaction effects and its influence on superconductivity. The question about the role of the electron-phonon coupling, which becomes specifically important since the superconductivity in $\text{La}_3\text{Ni}_2\text{O}_7$ is found under pressure, should also be clarified in future studies.

Conclusion.— In conclusion, we have introduced a minimal bilayer two-orbital model for the Ruddlesden-Popper bilayer $\text{La}_3\text{Ni}_2\text{O}_7$ under pressure. The tight-binding parameters are obtained by Wannier downfolding of the DFT calculations, which reproduce the band structure and Fermi surface well. The spin susceptibility is studied using the RPA method, which shows that the magnetic signal majorly comes from $d_{3z^2-r^2}$. This

model provides important means to the study of electronic, magnetic, orbital, and superconducting properties of the material under pressure.

We thank the useful discussions with Guang-Ming Zhang and Biao Lv. Work at Sun Yat-Sen University was supported by the National Key Research and Development Program of China (Grants No. 2022YFA1402802, 2018YFA0306001), the National Natural Science Foundation of China (Grants No. 92165204, No.12174454, No. 11974432, No.12274472), the Guangdong Basic and Applied Basic Research Foundation (Grants No. 2022A1515011618, No. 2021B1515120015), Guangdong Provincial Key Laboratory of Magnetoelectric Physics and Devices (Grant No. 2022B1212010008), Shenzhen International Quantum Academy (Grant No. SIQA202102), and Leading Talent Program of Guangdong Special Projects (201626003).

* These authors contributed equally to this work

† yaodaax@mail.sysu.edu.cn

- [1] H. Sun, M. Huo, X. Hu, J. Li, Y. Han, L. Tang, Z. Mao, P. Yang, B. Wang, J. Cheng, *et al.*, Superconductivity near 80 kelvin in single crystals of $\text{La}_3\text{Ni}_2\text{O}_7$ under pressure, [arXiv:2305.09586 \(2023\)](#).
- [2] J. G. Bednorz and K. A. Müller, Possible high T_c superconductivity in the Ba-La-Cu-O system, *Zeitschrift für Physik B Condensed Matter* **64**, 189 (1986).
- [3] P. W. Anderson, The resonating valence bond state in La_2CuO_4 and superconductivity, *Science* **235**, 1196 (1987).
- [4] P. A. Lee, N. Nagaosa, and X.-G. Wen, Doping a mott insulator: Physics of high-temperature superconductivity, *Rev. Mod. Phys.* **78**, 17 (2006).
- [5] B. Keimer, S. A. Kivelson, M. R. Norman, S. Uchida, and J. Zaanen, From quantum matter to high-temperature superconductivity in copper oxides, *Nature* **518**, 179 (2015).
- [6] H. Sakakibara, K. Suzuki, H. Usui, S. Miyao, I. Maruyama, K. Kusakabe, R. Arita, H. Aoki, and K. Kuroki, Orbital mixture effect on the fermi-surface- T_c correlation in the cuprate superconductors: Bilayer vs. single layer, *Phys. Rev. B* **89**, 224505 (2014).
- [7] W. Li, J. Zhao, L. Cao, Z. Hu, Q. Huang, X. Wang, Y. Liu, G. Zhao, J. Zhang, Q. Liu, *et al.*, Superconductivity in a unique type of copper oxide, *Proceedings of the National Academy of Sciences* **116**, 12156 (2019).
- [8] S. Raghu, X.-L. Qi, C.-X. Liu, D. J. Scalapino, and S.-C. Zhang, Minimal two-band model of the superconducting iron oxypnictides, *Phys. Rev. B* **77**, 220503 (2008).
- [9] A. V. Chubukov, D. V. Efremov, and I. Eremin, Magnetism, superconductivity, and pairing symmetry in iron-based superconductors, *Phys. Rev. B* **78**, 134512 (2008).
- [10] H. Eschrig and K. Koepf, Tight-binding models for the iron-based superconductors, *Phys. Rev. B* **80**, 104503 (2009).
- [11] M. Daghofer, A. Nicholson, A. Moreo, and E. Dagotto, Three orbital model for the iron-based superconductors, *Phys. Rev. B* **81**, 014511 (2010).

- [12] D. Li, K. Lee, B. Y. Wang, M. Osada, S. Crossley, H. R. Lee, Y. Cui, Y. Hikita, and H. Y. Hwang, Superconductivity in an infinite-layer nickelate, *Nature* **572**, 624 (2019).
- [13] E. Been, W.-S. Lee, H. Y. Hwang, Y. Cui, J. Zaanen, T. Devereaux, B. Moritz, and C. Jia, Electronic structure trends across the rare-earth series in superconducting infinite-layer nickelates, *Phys. Rev. X* **11**, 011050 (2021).
- [14] K.-W. Lee and W. E. Pickett, Infinite-layer LaNiO_2 : Ni^{1+} is not Cu^{2+} , *Phys. Rev. B* **70**, 165109 (2004).
- [15] M. Hepting, D. Li, C. Jia, H. Lu, E. Paris, Y. Tseng, X. Feng, M. Osada, E. Been, Y. Hikita, *et al.*, Electronic structure of the parent compound of superconducting infinite-layer nickelates, *Nature materials* **19**, 381 (2020).
- [16] A. S. Botana and M. R. Norman, Similarities and differences between LaNiO_2 and CaCuO_2 and implications for superconductivity, *Phys. Rev. X* **10**, 011024 (2020).
- [17] X. Wu, D. Di Sante, T. Schwemmer, W. Hanke, H. Y. Hwang, S. Raghu, and R. Thomale, Robust $d_{x^2-y^2}$ -wave superconductivity of infinite-layer nickelates, *Phys. Rev. B* **101**, 060504 (2020).
- [18] M. Jiang, M. Berciu, and G. A. Sawatzky, Critical nature of the Ni spin state in doped NdNiO_2 , *Phys. Rev. Lett.* **124**, 207004 (2020).
- [19] L.-H. Hu and C. Wu, Two-band model for magnetism and superconductivity in nickelates, *Phys. Rev. Res.* **1**, 032046 (2019).
- [20] Y. Nomura, M. Hirayama, T. Tadano, Y. Yoshimoto, K. Nakamura, and R. Arita, Formation of a two-dimensional single-component correlated electron system and band engineering in the nickelate superconductor NdNiO_2 , *Phys. Rev. B* **100**, 205138 (2019).
- [21] Y.-H. Zhang and A. Vishwanath, Type-II $t-j$ model in superconducting nickelate $\text{Nb}_{1-x}\text{Sr}_x\text{NiO}_2$, *Phys. Rev. Res.* **2**, 023112 (2020).
- [22] P. Werner and S. Hoshino, Nickelate superconductors: Multiorbital nature and spin freezing, *Phys. Rev. B* **101**, 041104 (2020).
- [23] F. Bernardini, V. Olevano, and A. Cano, Magnetic penetration depth and T_c in superconducting nickelates, *Phys. Rev. Res.* **2**, 013219 (2020).
- [24] Y. Gu, S. Zhu, X. Wang, J. Hu, and H. Chen, A substantial hybridization between correlated Ni-d orbital and itinerant electrons in infinite-layer nickelates, *Communications Physics* **3**, 84 (2020).
- [25] M. Kitatani, L. Si, O. Janson, R. Arita, Z. Zhong, and K. Held, Nickelate superconductors—a renaissance of the one-band hubbard model, *npj Quantum Materials* **5**, 59 (2020).
- [26] F. Lechermann, Doping-dependent character and possible magnetic ordering of NdNiO_2 , *Phys. Rev. Mater.* **5**, 044803 (2021).
- [27] A. Kreisel, B. M. Andersen, A. T. Rømer, I. M. Eremin, and F. Lechermann, Superconducting instabilities in strongly correlated infinite-layer nickelates, *Phys. Rev. Lett.* **129**, 077002 (2022).
- [28] F. Lechermann, Multiorbital processes rule the $\text{Nb}_{1-x}\text{Sr}_x\text{NiO}_2$ normal state, *Phys. Rev. X* **10**, 041002 (2020).
- [29] N. Kitamine, M. Ochi, and K. Kuroki, Designing nickelate superconductors with d^8 configuration exploiting mixed-anion strategy, *Phys. Rev. Res.* **2**, 042032 (2020).
- [30] G.-M. Zhang, Y.-f. Yang, and F.-C. Zhang, Self-doped mott insulator for parent compounds of nickelate superconductors, *Phys. Rev. B* **101**, 020501 (2020).
- [31] Z. Liu, H. Sun, M. Huo, X. Ma, Y. Ji, E. Yi, L. Li, H. Liu, J. Yu, Z. Zhang, *et al.*, Evidence for charge and spin density waves in single crystals of $\text{La}_3\text{Ni}_2\text{O}_7$ and $\text{La}_3\text{Ni}_2\text{O}_6$, *Science China Physics, Mechanics & Astronomy* **66**, 217411 (2023).
- [32] V. Pardo and W. E. Pickett, Metal-insulator transition in layered nickelates $\text{La}_3\text{Ni}_2\text{O}_{7-\delta}$ ($\delta = 0.0, 0.5, 1$), *Phys. Rev. B* **83**, 245128 (2011).
- [33] H. J. Choi, D. Roundy, H. Sun, M. L. Cohen, and S. G. Louie, The origin of the anomalous superconducting properties of MgB_2 , *Nature* **418**, 758 (2002).
- [34] M. Gao, Z.-Y. Lu, and T. Xiang, Prediction of phonon-mediated high-temperature superconductivity in $\text{Li}_3\text{B}_4\text{C}_2$, *Phys. Rev. B* **91**, 045132 (2015).
- [35] A. Drozdov, P. Kong, V. Minkov, S. Besedin, M. Kuzovnikov, S. Mozaffari, L. Balicas, F. Balakirev, D. Graf, V. Prakapenka, *et al.*, Superconductivity at 250 K in lanthanum hydride under high pressures, *Nature* **569**, 528 (2019).
- [36] M. Gao, Z. Lu, and T. Xiang, Finding high-temperature superconductors by metallizing the σ -bonding electrons, *PHYSICS* **44**, 421 (2015).
- [37] J. Hu, Identifying the genes of unconventional high temperature superconductors, *Science bulletin* **61**, 561 (2016).
- [38] J. Hu, C. Le, and X. Wu, Predicting unconventional high-temperature superconductors in trigonal bipyramidal coordinations, *Phys. Rev. X* **5**, 041012 (2015).
- [39] G. Kresse and J. Hafner, Ab initio molecular dynamics for liquid metals, *Phys. Rev. B* **47**, 558 (1993).
- [40] G. Kresse and J. Furthmüller, Efficient iterative schemes for ab initio total-energy calculations using a plane-wave basis set, *Phys. Rev. B* **54**, 11169 (1996).
- [41] P. E. Böchl, Projector augmented-wave method, *Phys. Rev. B* **50**, 17953 (1994).
- [42] J. P. Perdew, K. Burke, and M. Ernzerhof, Generalized gradient approximation made simple, *Phys. Rev. Lett.* **77**, 3865 (1996).
- [43] G. P. *et al.*, Wannier90 as a community code: new features and applications, *Journal of Physics: Condensed Matter* **32**, 165902 (2020).
- [44] N. Marzari and D. Vanderbilt, Maximally localized generalized wannier functions for composite energy bands, *Phys. Rev. B* **56**, 12847 (1997).
- [45] I. Souza, N. Marzari, and D. Vanderbilt, Maximally localized wannier functions for entangled energy bands, *Phys. Rev. B* **65**, 035109 (2001).
- [46] A. Georges, L. d. Medici, and J. Mravlje, Strong correlations from hunds coupling, *Annual Review of Condensed Matter Physics* **4**, 137 (2013).
- [47] T. A. Maier and D. J. Scalapino, Pair structure and the pairing interaction in a bilayer hubbard model for unconventional superconductivity, *Phys. Rev. B* **84**, 180513 (2011).
- [48] M. Nakata, D. Ogura, H. Usui, and K. Kuroki, Finite-energy spin fluctuations as a pairing glue in systems with coexisting electron and hole bands, *Phys. Rev. B* **95**, 214509 (2017).
- [49] P. Löwdin, A Note on the Quantum-Mechanical Perturbation Theory, *The Journal of Chemical Physics* **19**, 1396 (2004).
- [50] F. C. Zhang and T. M. Rice, Effective hamiltonian for the superconducting cu oxides, *Phys. Rev. B* **37**, 3759

- (1988).
- [51] J. Hu and H. Ding, Local antiferromagnetic exchange and collaborative fermi surface as key ingredients of high temperature superconductors, *Scientific reports* **2**, 381 (2012).